Localization of RFID Tags by a Moving Robot, via Phase Unwrapping and Non-Linear Optimization

Anastasios Tzitzis, Spyros Megalou, Stavroula Siachalou, Tsardoulias G. Emmanouil, Athanasios Kehagias, Traianos V. Yioultsis, *Member, IEEE*, and Antonis G. Dimitriou, *Senior Member, IEEE*

Abstract—In this paper, we propose a new method for the localization of RFID tags, by deploying off-the-shelf RFID equipment on a robotic platform. The constructed robot is capable to perform Simultaneous Localization (of its own position) and Mapping (SLAM) of the environment and then locate the RFID tags around its path. The proposed method is based on properly treating the measured phase of the backscattered signal by each tag at the reader's antenna, located on top of the robot. More specifically, the measured phase samples are reconstructed, such that the 2π discontinuities are eliminated (phase-unwrapping). This allows for the formation of an optimization problem, which can be solved rapidly by standard methods. The proposed method is experimentally compared against the SAR/imaging methods, which represent the accuracy benchmark in prior-art, deploying off-the-shelf equipment. It is shown that the proposed method solves *exactly* the same problem as holographic-imaging methods, overcoming the grid-density constraints of the latter. Furthermore, the problem, being calculations-grid-independent, is solved orders of magnitude faster, allowing for the applicability of the method in real-time inventorying and localization. It is also shown that the state-of-the-art SLAM method, which is used for the estimation of the trace of the robot, also suffers from errors, which directly affect the accuracy of the RFID localization method. Deployment of reference RFID tags at known positions, seems to significantly reduce such errors.

Index Terms—RFID, localization, robotics, SLAM, optimization, phase unwrapping.

I. INTRODUCTION

THIS work aims at automatic inventorying and accurate, real-time localization, by deploying a moving robot (see Fig. 1). The robot carries RFID equipment (reader, antenna) and a combination of sensors (lidar, depth cameras) to perform Simultaneous Localization (of the robot) and Mapping (of the area); also known as SLAM, [1]. SLAM produces a metric representation of the environment, also known as Occupancy Grid Map [2] and utilizes scan matching to keep track of the robot's pose [3].

Lidar and cameras are used for the localization of the robot, while RFID technology is used for the localization of
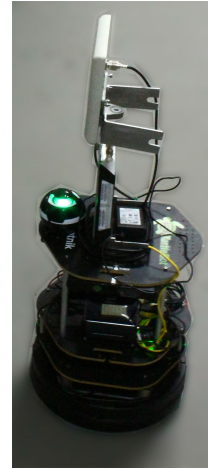
Fig. 1. SLAM and RFID enabled robot.

the objects in the surrounding (to the robot) environment. In contrast to optical technologies (e.g., camera), which require visual contact and advanced image-processing to identify objects, RFID technology exploits principles of RF. Passive RFID tags are attached to each object of interest. Each tag backscatters its unique ID, which is associated with the attached object. We wish to identify and locate the position of the tag. Representative applications could include warehouse-management or large retail stores. The proposed solution exploits ***mobility*** to reduce the overall cost of an equivalent inventorying solution, consisting of readers and antennas at fixed locations.

An additional advantage of mobility is the collection of many measurements for each tag, as the robot passes around its vicinity. Due to the absence of a battery source at the tag, a strong Line-Of-Sight (LOS) path is necessary for the activation of the tag's integrated circuit (IC), while other contributions from scatterers in the propagation area, are expected to be weaker [4]. The analysis in [4] indicates that the ratio of the power of the direct field to the mean of all other multipath is in the order of 8dBs-12dBs in the area within the reader-antenna's main lobe and is reduced to 4dBs at the vicinity of the surrounding walls. Depending on the above ratio, the phase of the LOS field, which is the essential information needed for accurate localization, is largely (for small ratios), or weakly (for large ratios) affected. This effect is shown in [5]. As the robot passes in the vicinity of the tag, it identifies the tag at successive locations for a total trace in the order of 4m to 6m,

collecting hundreds of measurements, depending on the speed of the robot (1300 samples are collected when the robot moves at 5cm/s). Due to the large collection of measurements, local (or temporary) areas with strong multipath, are expected to affect less the accuracy of the estimations. This wealth of measurements collected by a single moving antenna is often called as "virtual antenna array" in related prior art.

Localization techniques exploit the measured phase and back-scattered power of each tag at the reader-antenna pair located on the robot. Depending on the treatment of this information, we have direction-finding techniques, [6]–[8], "fingerprinting" methods, [9], [10], "holographic" and Synthetic Aperture (SAR) based methods, [11]–[15], conditional probability based methods [21]–[25] and other techniques [26]. Some may involve custom RFID-readers, [10], [26], usually Software Defined Radio transceivers, or out-of-band emissions [26]. Among the techniques that promise best accuracy with commodity RFID hardware (off the shelf components) are those based on exploiting the phase of the backscattered electromagnetic (EM) field and mainly the holographic method, or its differential variations, [11]–[15]. The reason is that the "holographic" method is a maximum likelihood estimator; it attempts to locate the position (of the tag) that best matches a set of phase-measurements. However, due to the non-convexity of the cost-function, application of the method demands for exhaustive search of all possible tag locations on a calculations' grid. As a consequence, despite of its high accuracy (for a dense grid), the estimation time is prohibitive for installations, involving large tag populations, or aiming at real-time results.

The key contribution of this paper is that we change the set of phase observations in an equivalent to the "holographic" maximum-likelihood cost-function, in such manner that estimation is derived by standard optimization methods; i.e., steepest descent, Newton's, line search, trust region etc. To achieve that, we perform "phase unwrapping" on the measured samples, "correcting" the phases for each tag to take continuous values, instead of being constrained in 2π intervals. Then, a solution of the optimization problem is rapidly found, while the estimation accuracy is expected to be better, compared to the holographic, since the proposed algorithm finds the best pair of coordinates, regardless of the grid's density.

The second contribution is that we treat the tags' localization problem in conjuction with the SLAM problem. To the best of our knowledge, this is the first time that the actual problem is realistically treated; both the poses of the robot (i.e., the reader-antennas) and the tags are unknown and must be evaluated. Prior-art treats those problems separately; RFID-tag localization algorithms consider the location of the reader-antenna as known, while SLAM algorithms aim only at localizing the robot (not the tags), apart from mapping the environment, [16]–[20]. It is found that the estimated robot's path from state-of-the-art SLAM methods suffers from significant errors, as will be demonstrated in Section IV. As a consequence, the tags' localization error increases accordingly. In this work, we attempt to correct those errors, by introducing reference tags at known locations.

We have constructed a prototype robot, demonstrated in Fig. 1. It is able to navigate autonomously in unknown environments, produce a map of them and track any object of interest therein. Experimental measurements verify the performance of the proposed method against the holographic approach. For a 2D search space, experimental results presented herein demonstrate a 55-times improvement in the estimation time of the proposed method with respect to the holographic. Assuming a 3D search space, the corresponding improvement would increase dramatically, since the holographic search-space would be multiplied to the size of the 3rd dimension, whereas in the proposed method, the estimation-time would not increase proportionally.

In Section II we present the problem. The proposed technique, named "Phase-ReLock", is presented in Section III. Experimental results are given in Section IV and conclusions at Section V.

II. DESCRIPTION OF THE PROBLEM

The robot moves along a straight path, e.g., inside a corridor, collecting measurements at l estimated locations with coordinates (x_i, y_i), $i = 1, l$. Consider that a tag t located at (x_t, y_t) is identified at $n \leq l$ antenna-locations. Let θ_{it} denote the phase measurement of the specific tag t at the ith antenna pose. The measured phase at the reader is proportional to the round-trip length of the reader-to-tag-to-reader link, plus a constant phase shift, introduced by the deployed hardware, [6].

A typical curve which represents the phase measured by a moving antenna is demonstrated in Fig. 2. The x-axis of the curve represents the x-coordinate of the robot's path. One can notice that the x-coordinate of the robot changes from 175cm to 750cm, since the specific tag was within reading-range of the antenna only during this part of the robot's trace. However, even in this part, there are substantial segments where the reader was not able to identify the tag, although the latter was in the reading-range of the antenna (e.g., from $x_i = 330cm$ to $x_i = 395cm$). Probably the signal did not exceed either the reader's or the tag's sensitivity, due to strong reflections at these regions of the environment.

One can also notice that the phase is wrapped in $[0, 2\pi)$ intervals, resulting in discontinuities every 2π. Within each interval, the phase reduces (the curve has negative slope) as the antenna-to-tag distance reduces, and then increases (positive slope) as the antenna-to-tag distance increases. When the slope of the curve changes sign ($x_i = 540cm$), the antenna-to-tag distance is minimized; the tag should be located at a line perpendicular to the robots trace, which crosses the (x_i, y_i) coordinates that correspond to the minimum of the phase curve.

Since the phase is measured in 2π intervals, the expected (theoretical) measurement at a readers antenna with coordinates (x_i, y_i), for a tag placed at (x_t, y_t) shall be

$$\phi_{it}(x_t, y_t, c_t) = \left(\frac{2\pi}{\lambda} 2d_{it} + c_t\right) \bmod 2\pi$$
$$= \left(\frac{4\pi}{\lambda}\sqrt{(x_t - x_i)^2 + (y_t - y_i)^2} + c_t\right) \bmod 2\pi,$$
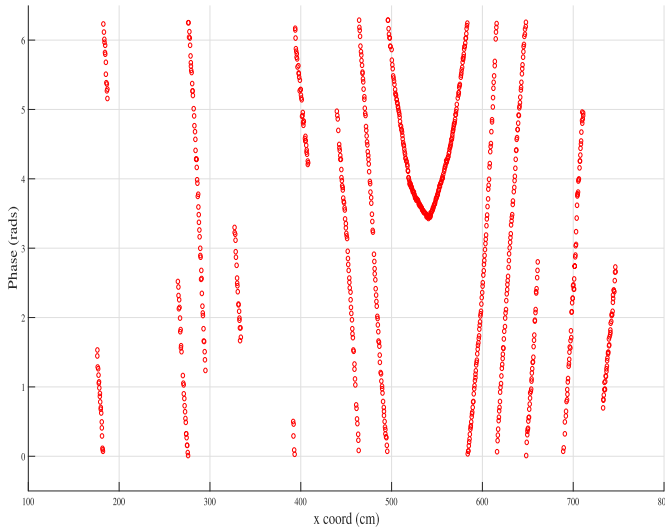$$i \in [1, n] \tag{1}$$

Fig. 2. Measured phase samples for a given tag.

assuming the problem is two-dimensional; in our set of experiments the reader's antenna was at the same height as the tags, which explains the absence of z coordinate in (1). c_t represents the constant phase shift introduced by the hardware to each measured sample of the tag t. We are searching for the possible tag coordinates for which the theoretical values ϕ_{it} calculated by (1) fit best to the measured samples θ_{it}; therefore, we need a cost function representing the deviation of the above two sets.

A. Holographic Imaging

The holographic method presented in [11] creates a cost function and performs an exhaustive search on all possible tag locations in the space of interest to find the one that best matches the observations/measurements. Let a grid of m possible locations of the unknown tag. For any possible location (x_k, y_k) of the grid the following cost function/term is calculated:

$$P_k = \left| \sum_{i=1}^{n} e^{j(\theta_{it} - \phi_{ik})} \right|, \quad k = 1, m \quad (2)$$

In (2), θ_{it} corresponds to the measured phase-sample of "target" tag t from the robot's coordinates (x_i, y_i) and ϕ_{ik} is the theoretical/expected phase value that would have been measured from the same robot's coordinates (x_i, y_i), if the tag was located at position (x_k, y_k). At a location near the actual tag position, these vectors are expected to add constructively, whereas at distant locations they will add randomly resulting in a much lower sum. According to this method, the coordinates of the tag are estimated by maximizing (2).

The cost function in (2) is slightly different in [12]–[15] to account for measurements collected by different antennas/ports; i.e., a phase subtraction from an initial sample per antenna-port is introduced in all measurements. An equivalent to (2) function is presented in [13]. According to it, the tag's estimated location is the grid's point for which the following

term is maximized:

$$C_k = \frac{|a_k^H b_t|^2}{\|a_k^H\|^2 \|b_t\|^2}, \quad k = 1, \ldots, m \quad (3)$$

where

$$a_k = \left[1, \ e^{-j(\phi_{2k} - \phi_{1k})}, \ldots, e^{-j(\phi_{nk} - \phi_{1k})}\right]^T, \quad k = 1, \ldots, m \quad (4)$$

and

$$b_t = \left[1, \ e^{-j(\theta_{2t} - \theta_{1t})}, \ldots, e^{-j(\theta_{nt} - \theta_{1t})}\right]^T. \quad (5)$$

However, the essence of the problem and the solution remains the same, demanding for a calculations-grid. For a dense grid, holographic methods are expected to ensure high accuracy, but can be time-consuming. The number of calculations involved is proportional to the size and density of the search space and for problems involving large unknown areas (as the ones our work targets) the estimation-time can be greatly increased.
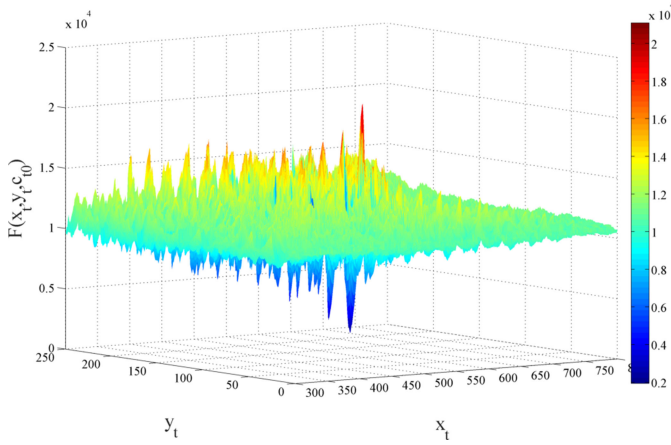
B. Proposed Method

Our goal is to fit the expected phase values calculated by (1) to the measured samples, by creating an appropriate cost/objective function, which can be optimized by standard optimization algorithms that promise rapid execution. Treating the above as an optimization problem, we are searching for the best selection of parameters (x'_t, y'_t, c'_t) that minimize the following function:

$$F(x_t, y_t, c_t) = \sum_{i=1}^{n} \left[\phi_{it}(x_t, y_t, c_t) - \theta_{it}\right]^2$$

$$= \sum_{i=1}^{n} \left[\left(\left(\frac{4\pi}{\lambda}\sqrt{(x_t - x_i)^2 + (y_t - y_i)^2} + c_t\right)\right.\right.$$

$$\left.\left. \times \mod 2\pi - \theta_{it}\right) \mod 2\pi\right]^2 \quad (6)$$

The pair (x'_t, y'_t) corresponding to the global minimum of (6) is the solution of the proposed algorithm.

The objective function (6) is nonlinear and should be minimized by applying a nonlinear optimization algorithm (e.g., [27]–[31]). Such algorithms are usually iterative. They start from an initial selection of the parameters and adjust them by exploiting certain information (e.g., the values of first or second derivatives), so that the objective function value decreases. The procedure shall be repeated until some specified convergence criteria are met. State-of-the-art nonlinear optimization algorithms are based on Steepest Descent direction, Newtons direction, Trust Region, etc. [32]. In general, such iterative algorithms converge to a local minimum of the objective function. However, optimization, by its definition, means finding the best solution overall and therefore ideally, algorithms should converge to the *global minimum*. This can be assured when convex objective functions are involved; i.e., functions with one and only global minimum

In our case, due to the repetitive form of both the curve of the expected phase values and the curve of the measured phase-samples, the objective function (6) tends to have a

Fig. 3.   Objective function $F(x_t, y_t, c_{t,0})$ for a constant $c_{t,0}$.

Fig. 4.   Objective function $F'(x_t, y_t, c_{t,0})$ for a constant $c_{t,0}$ after phase unwrapping.

repetitive-shaped surface, too, as shown in Fig. 3. As a consequence, it has many local minima (and maxima). The fitting algorithm will usually be trapped in a local minimum dependent on the initial point, instead of converging to the global minimum and finding the optimum solution.

III. PHASE RELOCK

We propose a post-processing of the phase measured samples so that the ***global minimum*** of the new objective function can be rapidly found by common optimization techniques. The proposed method is called **Phase ReLock** (**Loc(k)**alization by **Phase Re**construction). The processing of the samples refers to the reconstruction of the phase curve in order to obtain a continuous form, eliminating the discontinuities every 2π; this process is commonly known as ***phase-unwrapping***.
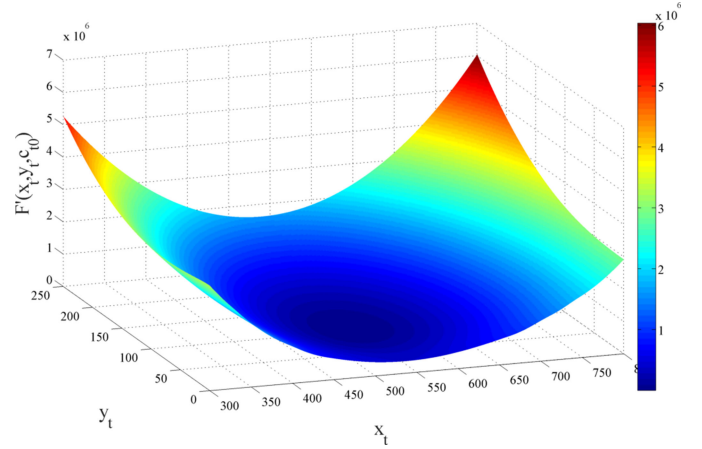
A. Creation of the Cost Function

Since our target is a continuous curve with no 2π jumps, the theoretical function (1) would have to change to:

$$\phi'_{it}(x_t, y_t, c_t) = \left(\frac{2\pi}{\lambda} 2d_{it} + c_t\right)$$
$$= \left(\frac{4\pi}{\lambda}\sqrt{(x_t - x_i)^2 + (y_t - y_i)^2} + c_t\right),$$
$$i = 1, \ldots, n \qquad (7)$$

and the new cost function would be written as:

$$F'(x_t, y_t, c_t)$$
$$= \sum_{i=1}^{n}\left[\phi'_{it}(x_t, y_t, c_t) - \theta'_{it}\right]^2$$
$$= \sum_{i=1}^{n}\left[\left(\frac{4\pi}{\lambda}\sqrt{(x_t - x_i)^2 + (y_t - y_i)^2} + c_t\right) - \theta'_{it}\right]^2 \quad (8)$$

where θ'_{it} is the processed/unwrapped phase sample corresponding to the "target" tag t measured at antenna's coordinates (x_i, y_i). One can notice that (7) and (8) are same as (1) and (6) respectively; the only difference being that the modulo operation has been removed. Furthermore, c_t here represents the number of whole cycles of phase offset between the unwrapped phase curve and the theoretical one,

plus the constant phase shift introduced by the deployed hardware.

The new objective function (8) no longer suffers from local minima as can be seen in Fig. 4. Therefore, an optimization algorithm can be applied to fit the expected values to the processed phase samples and find the optimum parameters (x'_t, y'_t, c'_t) that correspond to the global minimum of (8). The unknown location of the tag t is estimated as:

$$\left(x'_t, y'_t, c'_t\right) = \arg\min_{x_t, y_t, c_t} F'(x_t, y_t, c_t). \qquad (9)$$

B. Phase Unwrapping

1) Segmentation of the Set: As explained in Section II, whilst a tag is in reading-range of the reader, the reader could fail identifying it during some parts of its trace. As a result, the phase curve could contain segments with no samples at all. These segments indicate successive phase samples measured at relatively distant antenna's locations.

So initially, we divide the phase-curve into segments, so that each of them contains a set of samples taken at successive closely-spaced antenna's locations, as shown in Fig. 5 (a). We consider $\mathbf{\Theta}_j$ the set of the phase samples corresponding to the jth out of m created segments.

2) Unwrapping of Each Segment: For each segment we detect the discontinuities of the phase and distinguish every 2π interval in it. Let $\mathbf{\Theta}_{ij}$ be the set of the phase samples corresponding to the ith out of n 2π intervals of the jth segment. Each $\mathbf{\Theta}_{ij}$ represents a 2π part of the phase-curve of the specific segment, as shown in Fig. 6-top (where the 5th out of 7 segments is illustrated) and should be shifted along the phase-axis according to:

$$\mathbf{\Theta}'_{ij} = \mathbf{\Theta}_{ij} + 2\pi k_{ij}, \quad i = 1, \ldots, n. \qquad (10)$$

$k_{ij} \in Z$ and it's calculated so that a continuous curve is produced and any discontinuity between successive measurements is eliminated. Since in each segment the measurements are dense and successive phase samples correspond to closely-spaced robot's locations, one can expect that every 2π part should be placed at the end of the previous one, as shown in Fig. 6 - bottom. After the above procedure is repeated for
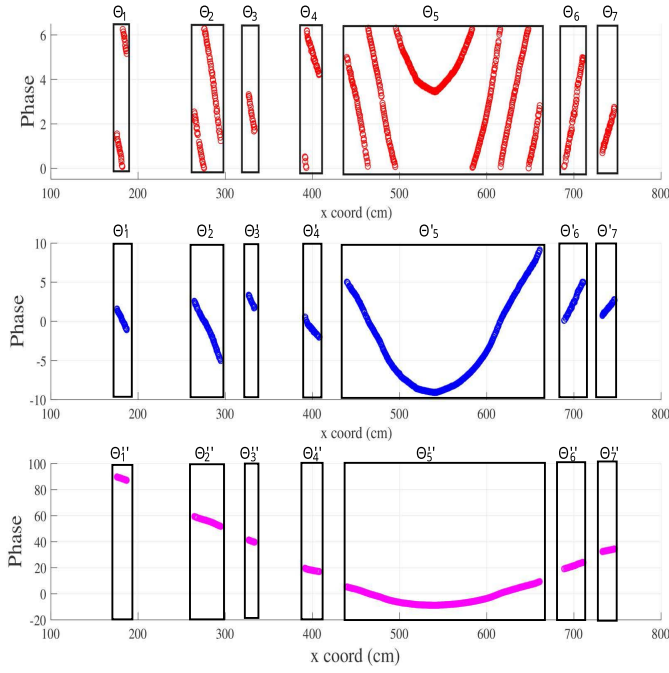
Fig. 5.   (a) Segmentation of the set - (b) Unwrapping of each segment independently - (c) Final step of the unwrap process.
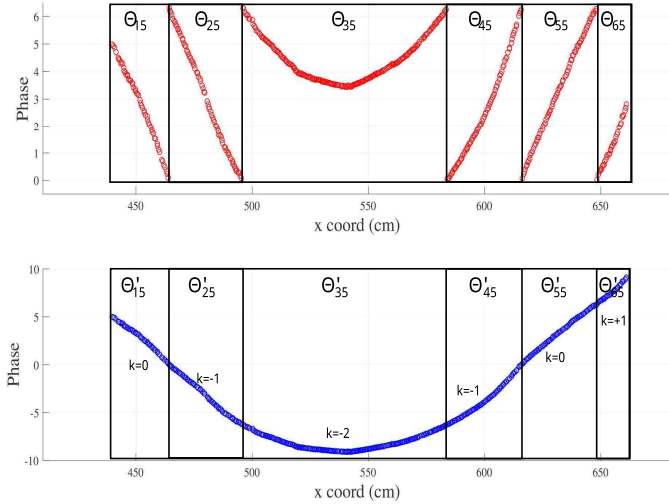

Fig. 6.   Unwrapping of the 5th segment.

every segment/set $\mathbf{\Theta}_j$ independently, the phase-curve is shown in Fig. 5 (b).

3) Unwrapping of Whole Set: The final part of phase-unwrapping aims to add the appropriate $2\pi \cdot k_j$ to each of the m **discontinuous** segments, such that the entire phase-set is unwrapped. Let $\mathbf{\Theta}'_j$ be the set of the processed phase samples corresponding to the jth out of m segments, consistently with the notation $\mathbf{\Theta}_j$ of Section III-B1. Each $\mathbf{\Theta}'_j$ should be shifted as before, according to

$$\mathbf{\Theta}''_j = \mathbf{\Theta}'_j + 2\pi k_j, \ j = 1, \dots, m. \quad (11)$$

The difficulty here arises from the fact that the successive segments $\mathbf{\Theta}'_j$ are not contiguous but are far apart. So, in contrast to the previous case when we had dense and
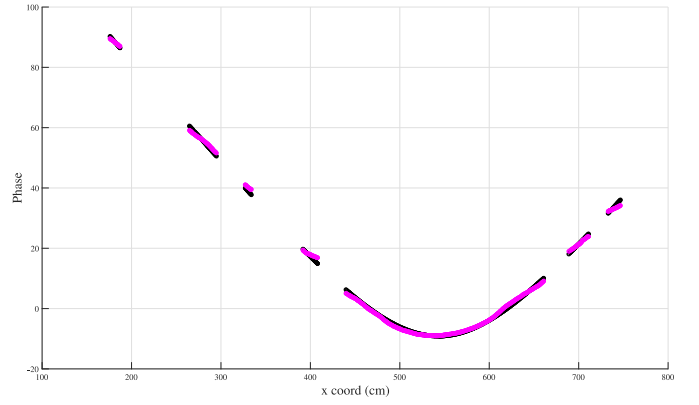

Fig. 7.   Unwrapped phase-curve (purple) vs. Phase ReLock theoretical phase-curve for optimum parameters (black).

closely-spaced sets of samples (i.e., Θ_{ij}), now the intervened periods of missing data result in an ambiguity regarding the true value of k_j. Theoretically, one should include each k_j, $j \in [1, m]$ as optimization parameter and select the solution $\{x_t, y_t, c_t, k_1, \dots, k_m\}$ that minimizes (8). This would greatly increase the computational time of the problem. Instead, in order to select the proper $k_j \cdot 2\pi$ per segment, we apply an iterative process, minimizing (8) and adding a single segment (to the previous iteration) each time, as described next.

The iterative process begins with the segment of the curve, where the slope's sign changes (the 5th one in the example of Fig. 5 (c)), because the phase-minimum also corresponds to the minimum robot-to-tag distance; hence one expects the power to be maximized at this part, having a strong LOS link. In order to detect such change, we further split each $\mathbf{\Theta}'_j$ into smaller parts (windows) and calculate their slopes (i.e., derivatives). A positive derivative indicates a window with increasing phase, whilst a negative derivative corresponds to decreasing phase and an alternation from negative to positive slope indicates a minimum robot-to-tag distance. Calculating derivatives of large parts instead of successive measurements reduces the phase-noise effect, since abrupt changes of slope may occur between adjacent samples, due to phase-noise. The segment in which an alternation from negative to positive slope occurs is the initial segment.

By applying (9) only for the initial segment, we get the first estimation of parameters x_t^0, y_t^0, c_t^0. Then we introduce another "target" segment $\mathbf{\Theta}'_j$ (e.g., $\mathbf{\Theta}'_6$). Given now the initial estimation of the parameters (x_t^0, y_t^0, c_t^0), we compute the theoretical unwrapped phase that should have been measured at the antenna's locations of the "target" segment, according to (7) for the previously estimated parameters. Let $\mathbf{\Phi}_j$ denote the set of these theoretical values. Then, an initial estimation of $k_j \in N$ of (11) is derived by:

$$k_j^{init} = \lfloor \overline{\left(\mathbf{\Theta}'_j - \mathbf{\Phi}_j \right)} / 2\pi \rceil, \quad j = 1, \dots, m \quad (12)$$

where $\overline{a}$ denotes the mean value of array a and $\lfloor b \rceil$ the nearest integer to b.

Equation (12) gives the best value of k_j, under the assumption that the tag is at the estimated coordinates (x_t^0, y_t^0), resulted from the initial segment. This is not necessarily the best overall solution but an indication that the best solution is around k_j^{init}.
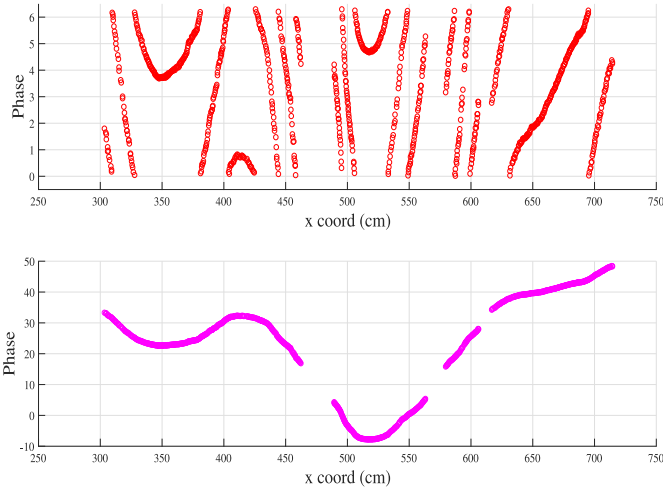
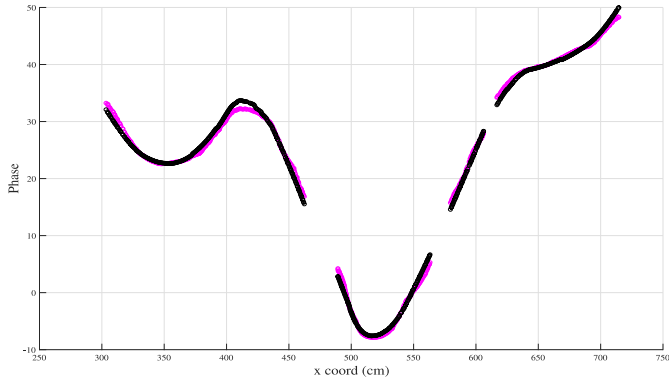Fig. 8. Unwrapping of the phase curve for non straight robot's trace.

Fig. 9. Unwrapped phase-curve (purple) vs. Phase ReLock theoretical phase-curve for optimum parameters (black) for non straight robot's trace.

Fig. 10. Representation of the measurements set-up corresponding to a straight path with "obstacles", where dielectric-boxes block some of the RFID tags. The target tags are arranged on top of a bench on a millimeter paper, so that their exact location can be compared against the results of Phase ReLock.

The final reconstructed/unwrapped phase curve is demonstrated in Fig. 5(c) and compared with the expected phase from the best x_t, y_t, c_t solution in Fig. 7.

C. Non Straight Paths

The robot is not expected to move on a straight-line, since it is configured to avoid obstacles, like people. An example of the phase-curve that corresponds to a slalom-type trajectory of the robot, including discontinuities within the segments, is demonstrated in Fig. 8-top. Phase ReLock can be applied for non straight robot's paths in the same manner, and the unwrapped phase is shown in Fig. 8-bottom. One can notice that the curve changes slope more than once, in contrast to cases of straight paths. This property necessitates a small change in the selection of the initial segment in the iterative process of phase-unwrapping of discontinuous segments. The algorithm starts from the segment, where the slope changes sign, from negative to positive. If two or more segments satisfy this condition, the algorithm selects the segment, where the mean power per sample is higher, signifying a smaller reader-to-tag distance. The result of Phase ReLock is presented in Fig. 9.

IV. EXPERIMENTAL RESULTS

A. Implementation

Measurements were performed, by constructing the robot, shown in Fig. 1. We used a Turtlebot2 [33] with a Kobuki

Therefore, for each $k_j \in [k_j^{init} - 1, k_j^{init} + 1]$ we shift Θ'_j according to (11), and re-apply (9) taking into consideration both introduced segments (i.e., the initial and the "target" one). For each of the above three candidate values k_j, an estimation of (x_t, y_t, c_t) is derived by (9). The final value of k_j is the one for which the amplitude of (8) is lowest. This is the "best" k_j and is used for the unwrapping process in (11).

At the end of this iteration, we have properly shifted a "target" segment Θ''_j and have an updated estimation of the parameters, x_t^1, y_t^1, c_t^1 by having taken into account two segments. The solution from the previous iteration x_t^0, y_t^0, c_t^0 represents the initial conditions (starting point for the optimization algorithm) of the updated estimations. The algorithm converges rapidly, as it always starts from the "best" previous solution. The robot's path during the missing periods is not involved anywhere in this process, since we need only the phase and the antenna's coordinates of the target segment. This process is repeated until all segments Θ'_j are properly shifted by the above procedure and an estimation of the unknown parameters is derived by (9) for the whole set of unwrapped data. This final estimation is the proposed solution of the localization problem.

Fig. 11.   Trajectories of the robot, estimated by the SLAM algorithm.

Fig. 12.   Map of the environment, created by the Mapping algorithm deployed in the robot, using the laser sensor located on top of it. The location of the robot, shown on the map is the estimated one at the specific time by the implemented particle-filter localization algorithm within SLAM.

mobile base [34] for motion support, appropriately equipped to perform both RFID localization and SLAM. It carries a 7dBic MT242032/NRH circularly polarized antenna from MTI Wireless Edge [35], connected to the Speedway Revolution R420 RFID reader [36], while the sensors responsible for the SLAM operations are an RPLidar A1 [37] and an Xtion Live Pro depth camera [38]. An Intel i7 CPU is attached to a MiniITX motherboard and an SSD drive for data storage.

The experiments took place in a long corridor-type laboratory room inside the campus (see Fig. 10) and were carried out in two phases. The first phase corresponds to the operation of SLAM; the robot traverses the "a priori" unknown space and creates a map of the environment (see Fig. 12) by exploiting sensor data and utilizing state-of-the-art SLAM algorithms, (e.g., [16], [17]). In the second phase, the robot moves along any trajectory and evaluates its position in the previously produced map. Concurrently, it continuously interrogates the RFID tags. The latter are placed at a millimeter-paper, forming a grid on the laboratory bench next to the wall. The locations of the tags on the millimeter paper are known exactly and are used for performance evaluation of the proposed localization method. The second phase was repeated 12 times for different robot's speeds and paths (see Fig. 11), while in some experiments, dielectric boxes were placed to block the LOS path between the antenna and those tags (see Fig. 10). The robot traversed different paths in order to accumulate different multipath in each measurement; the idea here was to have different distances from the opposite to the reader-antenna wall, so that no fixed maxima and minima of the field would be created. Five of the twelve paths are shown in Fig. 11, as the remaining trajectories were the same, but different speeds and/or obstacles were deployed. The trajectories shown in Fig. 11 represent the estimations of the SLAM algorithm; notice the discontinuities along each trajectory.

As soon as the experimental implementation was finished, we compared the holographic methods [11], [13] against the proposed "Phase ReLock". The holographic methods were executed for a limited space around the bench; a grid of $10m$ length and $2.5m$ width with $1cm$ grid-spacing. As for
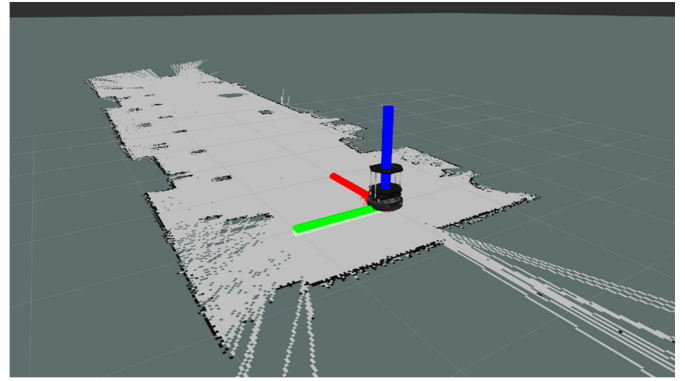
Phase ReLock, the optimization algorithm applied herein is a trust-region algorithm presented in [28] and [29].

B. Simultaneous Localization and Mapping - SLAM

During the first phase, where the environmental perception is being created, the SLAM algorithm used was Critical Rays Scan Matching (CRSM) SLAM [16]. CRSM is a scan-matching SLAM which does not utilize odometry in order to keep track of the robot's correct pose, i.e., the only sensor employed is a Lidar. CRSM acquires a lidar scan and performs a scan-to-map matching, i.e., it computes the 2D geometrical transformation that best aligns the current scan with the obstacles in the already existent map, whose reverse transformation is essentially the robot's translation and rotation. The difference of CRSM SLAM in comparison to other scan matching algorithms is that it automatically identifies which rays are the most important for the procedure (i.e., which are critical) and utilizes only them in the matching procedure, so as to be faster. The result is a metric map (see Fig. 12), also known as an OGM (Occupancy Grid Map), comprised of individual cells, each of which represents a portion of the space and holds the probability of this portion being occupied.

In the second phase, the already generated OGM is being used in order for the robot to localize itself. The robot localization algorithm used is AMCL (Adaptive Monte Carlo Localization) [17]. AMCL uses a particle filter to represent the robot pose's multimodal probabilistic distribution, where each particle contains an assumption of the robot's 2D pose. AMCL comprises two steps, the first of which is the motion update and the second is the sensor update. During the motion update, the particles' poses are updated based on the robot's odometry. Thus the particle filter increases its uncertainty due to the odometry errors, whilst in the sensor update phase, the particles are tested against the real lidar measurements. The particles which best fit the current measurement are probabilistically kept for the next iteration.

The trajectories of Fig. 11 are the output of the particle filter algorithm applied in the second phase. Parts of the trajectories suffer from discontinuities and "trembling", although the robot kept moving in a stable and continuous manner. These
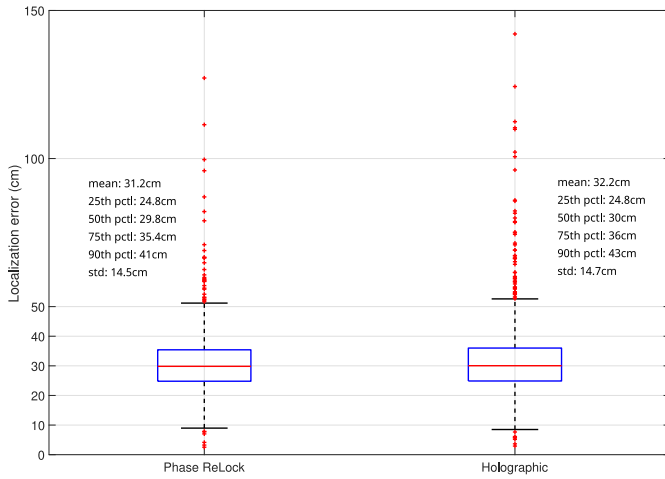
mean: 31.2cm
25th pctl: 24.8cm
50th pctl: 29.8cm
75th pctl: 35.4cm
90th pctl: 41cm
std: 14.5cm

mean: 32.2cm
25th pctl: 24.8cm
50th pctl: 30cm
75th pctl: 36cm
90th pctl: 43cm
std: 14.7cm

Fig. 13. Comparison between Phase ReLock and Holographic/SAR methods, including percentile errors.

Fig. 14. Performance of Phase ReLock vs robot's speed, assuming higher speeds.

discontinuities occur due to the nature of the particle filter algorithm applied for SLAM. This cause of error is irrelevant to the tag's localization method, but affects its accuracy.

C. Results

The locations of an average of 80 tags were estimated during each of the 12 experiments. The estimations were compared against the tags' actual coordinates on the millimeter paper. The estimations will accommodate all sources of errors: i) related to estimating the robots trace from the optical sensors and ii) related to the proposed method from the RFID-phase measurements.

The whole set of errors for the deployed methods corresponding to all estimations made, are shown in Fig. 13 in terms of percentiles. Since the cost functions in [11] and [13] are equivalent, they have the same accuracy and are represented by the same boxplot in Fig. 13. Similar accuracy between them and Phase ReLock is achieved.

Analytical results of each experiment are summarized in Table I. The mean error is comparable between Phase ReLock and the "holographic" methods, reporting a mean localization error slightly greater than 30cm. It should be noted that in some of the experiments Phase Relock performed slightly worse than the holographic methods; e.g., in the slalom trajectories 4 and 5. This is expected in experimental data, since the number of samples is finite and the mean error will not necessarily approximate the expected value, according to the law of large numbers. By calculating the total mean-error by all experiments, i.e., increasing the sample space, the overall accuracy of Phase ReLock is slightly better than the holographic methods, i.e., 1cm improvement; in the order of the calculation grid's spacing imposed by the latter.

It's also worth noting that in all three cases, where many of the tags were blocked, resulting in NLOS measured-samples, the accuracy of Phase-ReLock remained unaffected. Similar performance is recorded for the "slalom" paths of the robot.

More importantly, Phase ReLock has achieved a tremendous improvement of the algorithm's estimation-time. Whilst prior-art, [11], [13], required more than 20 minutes to locate an
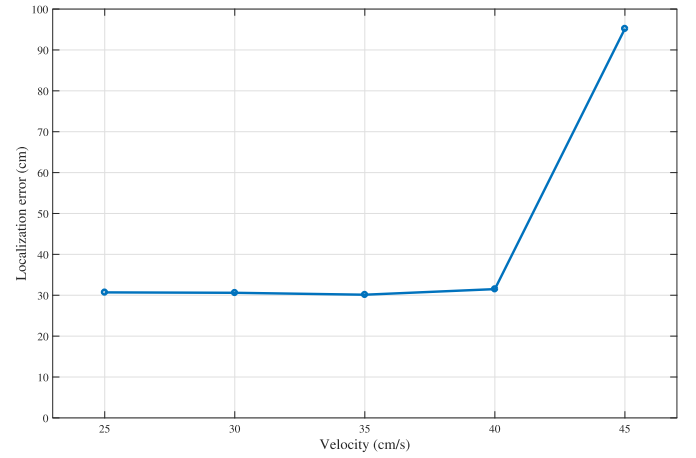
average of 80 tags, Phase ReLock performed 55 times faster and located all tags in less than 30s, requiring only 250ms per tag. This reduction-ratio would be further increased as the search space is increased, since the speed of the holographic depends on the size of the grid, whereas Phase ReLock doesn't. Actual cases demand larger grids since they are three-dimensional problems.

1) Performance vs Robot's Speed: Table I indicates that the deployed speeds of 5cm/s, 10cm/s and 20cm/s have similar performance; i.e., a mean error of 31cm. We validate the performance for increasing robot's speed by down-sampling the available data. For example, by taking 1 of every 5 samples of the data collected when the robot moves along path 2 at a speed of 5cm/s, the experiment becomes equivalent to moving at 5-times the original speed; i.e., 25cm/s for the same path. By repeating this process in 5cm/s speed increments, we evaluate the accuracy of Phase ReLock, as shown in Fig. 14. The accuracy is not affected for a speed up to 40cm/s, reporting a mean error around 30cm. Then, the error increases rapidly to 90cm, indicating failure of the method. The reason is that the number of samples per tag, collected within a 2π phase-interval are so few that phase-unwrapping fails. It should be noted that the maximum speed also depends on the number of tag-population within range. The larger the number of tags, the smaller the speed (since the slotted ALOHA access protocol of the tags will require for longer slot-periods to reduce the probability of collision). In our case, approximately 25 tags were within range during each interrogation phase.

D. SLAM Error and Correction

As aforementioned, the robot's trace is not known but estimated during SLAM. It is impossible for any SLAM algorithm to compute the robot's pose correctly at all times. Thus, the antenna's coordinates (x_i, y_i) involved in (7) and (8) introduce an additional error to any applied localization method, due to the false positioning of the robot. The actual deviation of the two paths for one of the experiments is shown in Fig. 15, where the estimated path (blue) never coincides with the actual one (green). Notice however that the two paths

TABLE I
EXPERIMENTAL RESULTS

|	Robot			Holographic/SAR methods [11], [13]			Phase ReLock		
path	velocity (cm/s)	distance from bench (cm)	obstacles blocking LOS	initial mean error (cm)	final mean error (cm)	estim-time (min)	initial mean error (cm)	final mean error (cm)	estim-time (min)
1	5	30	No	34.27	21.62	22.23	29.33	12.8	0.4
2	5	70	No	32.95	20.73	26.22	30.8	24.5	0.51
2	5	70	Yes	34.32	19.56	37.92	30.81	13.64	0.37
3	5	110	No	32.65	13.33	34.7	33.6	13.72	0.48
4	5	slalom	No	31.11	15.1	41.8	33.68	18.9	0.55
2	10	70	No	30.78	18.61	18.98	29.83	18	0.44
2	10	70	Yes	29.76	13.88	16.43	29.08	13.18	0.29
3	10	110	No	34.4	13.97	21.95	34	12.9	0.43
5	10	slalom	No	30	16.13	24.33	32.4	17.6	0.59
2	20	70	No	31.24	20.76	13.93	30.47	26.36	0.37
2	20	70	Yes	33.51	15.39	11.15	30.16	13.28	0.31
3	20	110	No	31.17	12.18	14.58	29.66	15.13	0.37
mean values				32.2	16.7	23.68	31.2	16.9	0.42
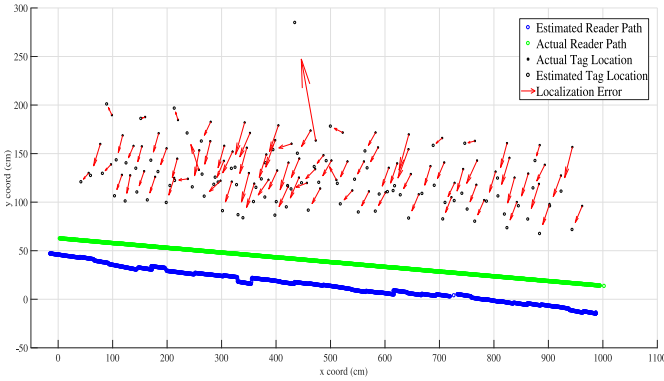
Fig. 15. Initial localization results, without correction of error, caused by SLAM.
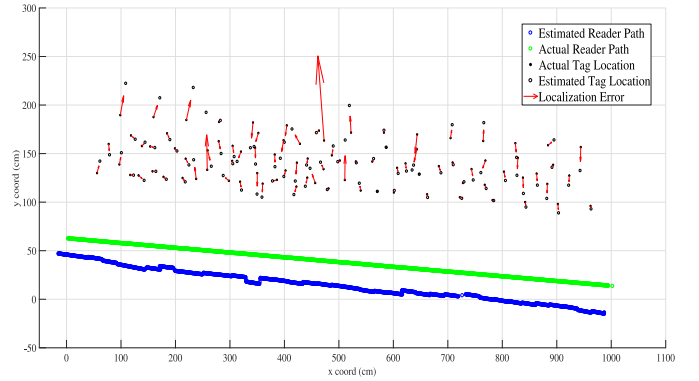

Fig. 16. Improved localization results, applying common error reduction, by deploying tags at known locations.

are parallel; causing a similar "common" error to the estimated locations of the tags. Estimated tags lay mainly on the southwest of the actual locations. Assuming that this kind of displacement/shifting of the robot's path affects the estimations of all tags in the same way by adding a common error, we attempt to improve the estimations by exploiting some tags with known coordinates.

By using only 8 tags as reference, and subtracting their x, y coordinates estimation error from all other tags, we correct the estimations for the entire set. The improvement is evident, as illustrated in Fig. 16 and presented in Table I. However, the selection and the location of the reference tags is of vital importance to this improvement, since a bad selection of reference tags, i.e., not representative of the common error, could have a negative impact on the correction (for this experiment, we have simply selected 8 tags along the center of the bench). Thanks to the low-cost of passive RFID-tags, one can deploy an arbitrarily large number of reference tags, to reduce the statistical risk of a poor sample. In general, correction of the error by reference tags is investigated here as a possibility. Concurrently, we aim the improvement of the SLAM algorithm (particle filtering algorithm), in order to minimize the errors regarding the robot's estimated trace.

The detailed results of the deployed methods for each experiment, before and after the correction, and the estimation-times are given in Table I. As far as accuracy is concerned, Phase Relock and the holographic methods are equivalent. They have both accomplished to locate the tags with an initial mean error of 31cm and 32cm respectively, while the correction of the estimations based on reference tags has reduced the error about by half, to 17cm each.

E. Source of Error

We identify the following causes of error: i) erroneous estimation of the locations the robot, ii) deformations of the actual map of the area, iii) multipath and iv) hardware introduced errors. The first error can be jointly corrected by improving the particle filter algorithm of SLAM, probably forcing the poses-update vector in the filter to block large steps and by deploying RFID tags at known locations, as applied herein. However, further work needs to be done, since this error could be local and variable across different regions; the corrections should be applied in smaller areas, while preserving continuity of the robot's trace in the resultant trajectory. The second error arises from transformations of the estimated map (which affects again the locations of

the robot); imagine an estimated "bent" map of the environment, which needs to be unbent in order to match the phase-measurements corresponding to the actual dimensions of the environment. Again, application of corrections by reference tags could be deployed. The third error, multipath, cannot be traced by the phase-measured samples alone. However, the reader also collects power measurements of the backscattered signal per tag. Possibly, from the power profile, areas that suffer from greater multipath can be identified and the measured phase samples can be excluded from the estimations. Further improvements are expected by deploying multiple antennas on top of the robot, forming new propagation conditions with the tags, allowing for selection of the best samples. Finally, the phase-measurements hardware error is of Gaussian nature and small [15] (0 mean, std 0.1 rad); hence the proposed method, treating a long series of samples will correct this error, thanks to its zero-mean property.

V. CONCLUSION

In this work, we have presented a novel localization method which solves the "holographic" problem exactly. The main contribution of this work, is the modification of the initial problem/optimization function, eliminating local minima, so that it can be solved by standard optimization techniques rapidly. The key to succeed is the introduction of a phase-unwrapping process. Experimental results validate the accuracy of the method. In contrast to related prior-art, the method is independent of any grid density and orders of magnitude faster; thus, it can be ideal for a trustworthy real-time inventorying and localization.

State-of-the-art localization algorithms, based on the holographic method, report accuracy below 5cm, e.g., [12], [14], but include multipath-reduction techniques involving multiple frequencies and multiple antennas, while they consider the robot-antenna positions as known. Such multipath-mitigation techniques can also be deployed with Phase ReLock, leading to at least the same accuracy, since we solve exactly the same problem, deployed therein. Hence, an estimation accuracy below 10cm is expected by accommodating multiple antennas and multiple frequencies.

In contrast to prior-art, we have considered the actual problem, where the robot must also locate itself in the map. As a result, the robot's self-localization error is "accumulated" to the localization error of the tags (since the reference positions of the reader are not exact). In fact, the error introduced by SLAM is comparable and sometimes larger than the RFID-related error. This can be reduced by exploiting tags at known locations, as shown herein.

REFERENCES

[1] C. Cadena *et al.*, "Past, present, and future of simultaneous localization and mapping: Toward the robust-perception age," *IEEE Trans. Robot.*, vol. 32, no. 6, pp. 1309–1332, Dec. 2016.

[2] A. Milstein, "Occupancy grid maps for localization and mapping," in *Motion Planning*. London, U.K.: InTech, Jun. 2008, pp. 381–408.

[3] A. Diosi and L. Kleeman, "Laser scan matching in polar coordinates with application to SLAM," in *Proc. IEEE/RSJ Int. Conf. Intell. Robots Syst.*, Dec. 2005, pp. 3317–3322.

[4] A. G. Dimitriou, S. Siachalou, A. Bletsas, and J. N. Sahalos, "A site-specific stochastic propagation model for passive UHF RFID," *IEEE Antennas Wireless Propag. Lett.*, vol. 13, pp. 623–626, 2014.

[5] T. Faseth, M. Winkler, H. Arthaber, and G. Magerl, "The influence of multipath propagation on phase-based narrowband positioning principles in UHF RFID," in *Proc. IEEE-APS Topical Conf. Antennas Propag. Wireless Commun. (APWC)*, Torino, Italy, 2011, pp. 1144–1147.

[6] P. V. Nikitin, R. Martinez, S. Ramamurthy, H. Leland, G. Spiess, and K. V. S. Rao, "Phase based spatial identification of UHF RFID tags," in *Proc. IEEE Int. Conf. RFID*, Orlando, FL, USA, 2010, pp. 102–109.

[7] J. Zhou, H. Zhang, and L. Mo, "Two-dimension localization of passive RFID tags using AOA estimation," in *Proc. IEEE Instrum. Meas. Technol. Conf. (I2MTC)*, Binjiang, China, 2011, pp. 1–5.

[8] S. Azzouzi, M. Cremer, U. Dettmar, R. Kronberger, and T. Knie, "New measurement results for the localization of UHF RFID transponders using an angle of arrival (AoA) approach," in *Proc. IEEE Int. Conf. RFID*, Orlando, FL, USA, 2011, pp. 91–97.

[9] L. M. Ni and Y. Liu, "LANDMARC: Indoor location sensing using active RFID," *Wireless Netw.*, vol. 10, no. 6, pp. 701–710, 2004.

[10] J. Wang and D. Katabi, "Dude, where's my card? RFID positioning that works with multipath and non-line of sight," in *Proc. ACM SIGCOMM Conf. SIGCOMM*, Hong Kong, 2013, pp. 51–62.

[11] R. Miesen, F. Kirsch, and M. Vossiek, "Holographic localization of passive UHF RFID transponders," in *Proc. IEEE Int. Conf. RFID*, Orlando, FL, USA, 2011, pp. 32–37.

[12] L. Shangguan and K. Jamieson, "The design and implementation of a mobile RFID tag sorting robot," in *Proc. 14th Annu. Int. Conf. Mobile Syst. Appl. Services*, 2016, pp. 31–42.

[13] A. Motroni *et al.*, "SAR-based indoor localization of UHF-RFID tags via mobile robot," in *Proc. Int. Conf. Indoor Position. Indoor Navig. (IPIN)*, Nantes, France, 2018, pp. 1–8.

[14] A. Motroni, P. Nepa, P. Tripicchio, and M. Unetti, "A multi-antenna SAR-based method for UHF RFID tag localization via UGV," in *Proc. IEEE Int. Conf. RFID Technol. Appl. (RFID-TA)*, Macau, China, 2018, pp. 1–3.

[15] L. Yang, Y. Chen, X.-Y. Li, C. Xiao, M. Li, and Y. Liu, "Tagoram: Real-time tracking of mobile RFID tags to high precision using cots devices," in *Proc. 20th Annu. Int. Conf. Mobile Comput. Netw.*, 2014, pp. 237–248.

[16] E. Tsardoulias and L. Petrou, "Critical rays scan match SLAM," *J. Intell. Robot. Syst.*, vol. 72, nos. 3–4, pp. 441–462, 2013.

[17] F. Dieter, W. Burgard, F. Dellaert, and S. Thrun, "Monte Carlo localization: Efficient position estimation for mobile robots," in *Proc. AAAI/IAAI*, 1999, pp. 343–349.

[18] M. Montemerlo, S. Thrun, D. Koller, and B. Wegbreit, "FastSLAM 2.0: An improved particle filtering algorithm for simultaneous localization and mapping that provably converges," in *Proc. 16th Int. Joint Conf. Artif. Intell.*, 2003, pp. 1151–1156.

[19] A. I. Eliazar and R. Parr, "DP-SLAM: Fast, robust simultaneous localization and mapping without predetermined landmarks," in *Proc. Int. Conf. Artif. Intell.*, Acapulco, Mexico, 2003, pp. 1135–1142.

[20] W. Hess, D. Kohler, H. Rapp, and D. Andor, "Real-time loop closure in 2D LIDAR SLAM," in *Proc. IEEE Int. Conf. Robot. Autom. (ICRA)*, Stockholm, Sweden, 2016, pp. 1271–1278.

[21] S. Siachalou, A. Bletsas, J. N. Sahalos, and A. G. Dimitriou, "RSSI-based maximum likelihood localization of passive RFID tags using a mobile cart," in *Proc. IEEE Wireless Power Transfer Conf. (WPTC)*, Aveiro, Portugal, 2016, pp. 1–4.

[22] S. Subedi, E. Pauls, and Y. D. Zhang, "Accurate localization and tracking of a passive RFID reader based on RSSI measurements," *IEEE J. Radio Freq. Identification*, vol. 1, no. 2, pp. 144–154, Jun. 2017.

[23] J. Zhang, Y. Lyu, J. Patton, S. C. G. Periaswamy, and T. Roppel, "BFVP: A probabilistic UHF RFID tag localization algorithm using Bayesian filter and a variable power RFID model," *IEEE Trans. Ind. Electron.*, vol. 65, no. 10, pp. 8250–8259, Oct. 2018.

[24] F. Martinelli, "A robot localization system combining RSSI and phase shift in UHF-RFID signals," *IEEE Trans. Control Syst. Technol.*, vol. 23, no. 5, pp. 1782–1796, Sep. 2015.

[25] P. Yang and W. Wu, "Efficient particle filter localization algorithm in dense passive RFID tag environment," *IEEE Trans. Ind. Electron.*, vol. 61, no. 10, pp. 5641–5651, Oct. 2014.

[26] Y. Ma, N. Selby, and F. Adib, "Minding the billions: Ultra-wideband localization for deployed RFID tags," in *Proc. 23rd Annu. Conf. Mobile Comput. Netw. (MobiCom)*, 2017, pp. 248–260.

[27] M. A. Branch, T. F. Coleman, and Y. Li, "A subspace, interior, and conjugate gradient method for large-scale bound-constrained minimization problems," *SIAM J. Sci. Comput.*, vol. 21, no. 1, pp. 1–23, 1999.

[28] R. H. Byrd, R. B. Schnabel, and G. A. Shultz, "Approximate solution of the trust region problem by minimization over two-dimensional subspaces," *Math. Program.*, vol. 40, nos. 1–3, pp. 247–263, 1988.

[29] J. J. Moré and D. C. Sorensen, "Computing a trust region step," *SIAM J. Sci. Stat. Comput.*, vol. 4, no. 3, pp. 553–572, 1983.

[30] D. W. Marquardt, "An algorithm for least-squares estimation of nonlinear parameters," *SIAM J. Appl. Math.*, vol. 11, no. 2, pp. 431–441, 1963.

[31] K. Levenberg, "A method for the solution of certain problems in least squares," *Quart. Appl. Math.*, vol. 2, no. 2, pp. 164–168, 1944.

[32] V. Buljak, "Optimization algorithms," in *Inverse Analyses With Model Reduction*, 1st ed. Berlin, Germany: Springer, 2012, pp. 19–83.

[33] *Turtlebot 2 Platform*. Accessed: Oct. 10, 2018. [Online]. Available: http://www.turtlebot.com/turtlebot2/

[34] *Kobuki Mobile Base*. Accessed: Oct. 10, 2018. [Online]. Available: http://kobuki.yujinrobot.com/

[35] *MTI Wireless Edge LTD*. Accessed: Oct. 10, 2018. [Online]. Available: http://www.mtiwe.com/

[36] *Impinj R420 RFID Reader*. Accessed: Oct. 10, 2018. [Online]. Available: https://https://www.impinj.com/platform/connectivity/speedway-r420/

[37] *RPLidar Sensor*. Accessed: Oct. 10, 2018. [Online]. Available: https://www.slamtec.com/en/Lidar/A1

[38] *Xtion Live Pro Depth Camera*. Accessed: Oct. 10, 2018. [Online]. Available: https://www.asus.com/gr/3DSensor/Xtion_PRO_LIVE/

Tsardoulias G. Emmanouil received the Engineering Diploma and Doctoral degrees from the Department of Electrical and Computer Engineering, Aristotle University of Thessaloniki (AUTH), Greece, in 2007 and 2013, respectively. His working experience includes participation in the Eudoxus Project with the collaboration of Ministry of Education, the EU Project RAPP (FP7-ICT-610947), and NSRF Projects (RELIEF, TekTrain, and SYTHES) among others. His research interests are focused on robotics and specifically in autonomous robots (ground or aerial). Some of the topics involved are autonomous navigation, simultaneous localization and mapping, multirobot exploration/full coverage, and robotic architectures oriented for the creation of robotic applications and robot-agnostic RESTful APIs. Since 2009, he has been a Technical Manager of the Artificial Intelligence Group, P.A.N.D.O.R.A. and R4A robotics teams, which operate with the School of Electrical and Computer Engineering, Aristotle University of Thessaloniki. PANDORA has participated in five world-wide RoboCup competitions, achieving the second place in the Autonomy finals twice.

Athanasios Kehagias received the Diploma degree in electrical engineering from the Aristotle University of Thessaloniki, Greece, in 1984, the M.Sc. degree in applied mathematics from Lehigh University, Bethlehem, PA, USA, in 1985, and the Ph.D. degree in applied mathematics from Brown University, Providence, RI, USA, in 1991. Since 2012, he has been an Associate Professor of applied mathematics with the Department of Electrical and Computer Engineering, Aristotle University of Thessaloniki. His research interests include stochastic processes, game theory, and fuzzy sets.

Traianos V. Yioultsis (M'09) received the Diploma and Ph.D. degrees in electrical and computer engineering from the Aristotle University of Thessaloniki, Greece, in 1992 and 1998, respectively. From 2001 to 2002, he was a Post-Doctoral Research Associate with the Department of Electrical and Computer Engineering, University of Illinois at Urbana–Champaign. Since 2002, he has been with the Department of Electrical and Computer Engineering, Aristotle University of Thessaloniki, where he is currently a Professor. His current interests include the analysis and design of antennas and microwave circuits with fast computational techniques, and the modeling of complex wave propagation problems. He has also served as an Editorial Board Member for IEEE COMMUNICATIONS LETTERS and several international conferences.

Anastasios Tzitzis was born in Thessaloniki, Greece, in 1994. He received the Diploma degree in electrical and computer engineering from the Aristotle University of Thessaloniki in 2018, where he is currently pursuing the Ph.D. degree and concurrently a Research and Teaching Assistant. His current research interests include analysis and design of antennas, RFID technology, and wave propagation.

Spyros Megalou received the M.Sc. degree in electrical and computer engineering from the Aristotle University of Thessaloniki, Greece, in 2019, where he is currently pursuing the Ph.D. degree. His main research interests include RFID technology, localization techniques, microwave applications, and antenna design. He is also a member of a space-related group (Beyond Earth Aristotle Missions) focusing on space experiments and applications.
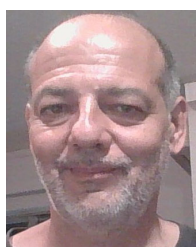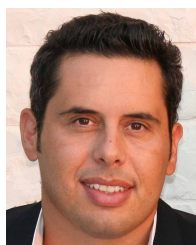

Antonis G. Dimitriou (S'01–M'06–SM'14) received the Diploma and Ph.D. degrees in electrical and computer engineering from the Aristotle University of Thessaloniki (AUTh), Greece, in 2001 and 2006, respectively.

Since 2007, he has been with the School of Electrical and Computer Engineering, AUTh, where he is currently a Teaching and Research Faculty Member. He has participated in over 20 research projects, 8 of which since 2007 as a Principal Investigator in the fields of robotics, RFIDs, and wireless sensor networks. He is currently the Coordinator of the Project RELIEF, where prototype simultaneous localization and mapping-capable terrestrial robots and drones are designed and constructed to continuously perform inventorying and localization of RFID-tagged items. He was a Management Committee Member in the ICT COST Action IC301 "Wireless Power Transmission for Sustainable Electronics." He has authored or coauthored approximately 60 journal and conference papers.

Dr. Dimitriou was a recipient of the Ericsson Award of Excellence in Telecommunications in 2001 and the "IEEE Wireless Communications Letters Exemplary Reviewer" Award in 2012 and 2014. He was a co-recipient of the Student-Paper Award in the 2011 IEEE RFID-TA conference. He also serves as a reviewer for major journals and a TPC member for international conferences.

Stavroula Siachalou received the Diploma and Ph.D. degrees in electrical and computer engineering from the Aristotle University of Thessaloniki (AUTh), Greece, in 2000 and 2005, respectively.

She is currently with the School of Electrical and Computer Engineering, AUTh, as a Teaching and Research Faculty Member. She has participated in several research projects in the fields of wireless communications and RFIDs. She has authored or coauthored over 20 journal and conference papers. Her research interests include information routing, dynamic resource allocation in wireless networks, RFIDs, and localization techniques. She also serves as a reviewer for major journals and conferences.